

# Reduced Spike-Timing Reliability Correlates with the Emergence of Fast Ripples in the Rat Epileptic Hippocampus

Guglielmo Foffani,<sup>2,5</sup> Yoryani G. Uzcategui,<sup>1,5</sup> Beatriz Gal,<sup>1,3</sup> and Liset Menendez de la Prida<sup>1,4,\*</sup>

<sup>1</sup>Neurobiología-Investigación, Hospital Ramón y Cajal, Madrid 28034, Spain

<sup>2</sup>Fundación del Hospital Nacional de Paraplégicos para la Investigación y la Integración, SESCAM, Toledo 45071, Spain

<sup>3</sup>Ciencias Morfológicas y Fisiología, Universidad Europea de Madrid, Madrid 28670, Spain

<sup>4</sup>Present address: Instituto Cajal - CSIC, Av. Doctor Arce 37, Madrid 28002, Spain.

<sup>5</sup>These authors contributed equally to this work.

\*Correspondence: [lmprida@cajal.csic.es](mailto:lmprida@cajal.csic.es)

DOI 10.1016/j.neuron.2007.07.040

## SUMMARY

Ripples are sharp-wave-associated field oscillations (100–300 Hz) recorded in the hippocampus during behavioral immobility and slow-wave sleep. In epileptic rats and humans, a different and faster oscillation (200–600 Hz), termed fast ripples, has been described. However, the basic mechanisms are unknown. Here, we propose that fast ripples emerge from a disorganized ripple pattern caused by unreliable firing in the epileptic hippocampus. Enhanced synaptic activity is responsible for the irregular bursting of CA3 pyramidal cells due to large membrane potential fluctuations. Lower field interactions and a reduced spike-timing reliability concur with decreased spatial synchronization and the emergence of fast ripples. Reducing synaptically driven membrane potential fluctuations improves both spike-timing reliability and spatial synchronization and restores ripples in the epileptic hippocampus. Conversely, a lower spike-timing reliability, with reduced potassium currents, is associated with ripple shuffling in normal hippocampus. Therefore, fast ripples may reflect a pathological desynchronization of the normal ripple pattern.

## INTRODUCTION

High-frequency oscillations of local field potentials have been reported in several brain structures under normal and pathological conditions (Kandel and Buzsáki, 1997; Jones and Barth, 1999; Foffani et al., 2003; Grenier et al., 2001; Traub et al., 2005). In the hippocampus, high-frequency oscillations termed ripples (100–300 Hz) are typically associated with sharp-wave (SPW) activity recorded during behavioral immobility and slow-wave sleep (Suzuki and Smith, 1988; Buzsáki et al., 1992; Wil-

son and McNaughton, 1994; Skaggs and McNaughton, 1996; O'Neill et al., 2006). SPW ripples originate from the synchronized firing of CA3 cells and propagate downstream (Ylinen et al., 1995; Csicsvari et al., 2000). In rats with recurrent spontaneous seizures, SPW-associated field oscillations are faster (200–600 Hz) and labeled fast ripples (Bragin et al., 1999, 2002). Fast ripples, which sometimes precede seizure onset (Jirsch et al., 2006; Khosravani et al., 2005), are found exclusively in epileptogenic regions (Bragin et al., 2002) and are suggested to reflect the pathological hypersynchronization of neuronal assemblies (Bragin et al., 2000). However, in spite of substantial work, the cellular and network processes underlying ripples and fast ripples remain elusive.

Here, we combine single-cell and circuit electrophysiology to examine the cellular mechanisms of ripples and fast ripples using an in vitro model of SPW (Kubota et al., 2003; Maier et al., 2003; Behrens et al., 2005) and the lithium-pilocarpine model of temporal lobe epilepsy. We show that the precise temporal relationship between single-cell firing and population ripples is disrupted in the hippocampus of epileptic rats. We propose that fast ripples are created by unreliable single-cell firing that is weakly correlated at the population level. Lower field interactions in the sclerotic hippocampus, together with reduced spike-timing reliability due to large synaptically driven membrane potential fluctuations, are associated with the emergence of fast ripples. Manipulations that indirectly improve spike-timing reliability deteriorate fast ripples and restore the ripple pattern in the epileptic hippocampus. Conversely, reducing spike-timing reliability in the control hippocampus by directly interfering with the delayed rectifier potassium current is associated with decreased spatial synchronization and shuffled ripple oscillations. We suggest that fast ripples reflect a pathological disruption of the normal ripple pattern in the hippocampus of epileptic rats.

## RESULTS

A total of 78 male Sprague-Dawley rats were used in this study. Thirty-three animals were made epileptic after

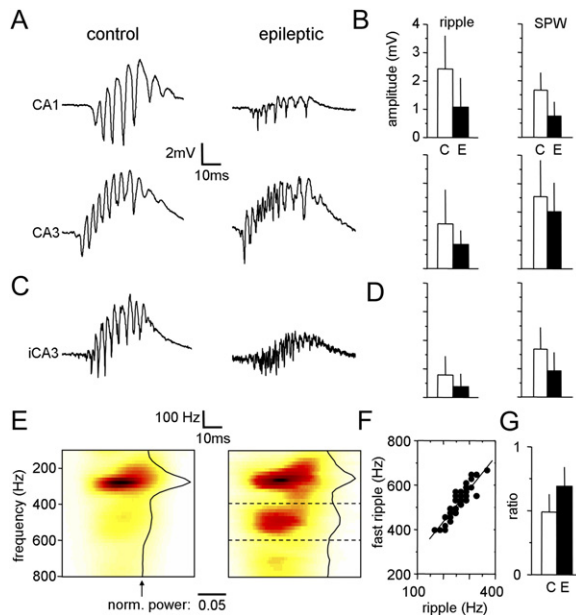


**Figure 1. Sharp Waves and Ripples Are Recorded in Conventional Hippocampal Slices from Normal and Epileptic Rats**

(A) Representative simultaneous field recordings from the CA3 and the CA1 regions in slices from control (left) and epileptic rats (right). Spontaneous SPW ripples were initiated in the CA3 area and propagated downstream. Fast ripples were evident in recordings from the epileptic hippocampus (right).

(B) The amplitude of ripples and SPWs in both regions was significantly different between control and epileptic rats ( $p < 0.05$ ).

(C) Ripples and fast ripples were recorded in the isolated CA3 area of control (left) and epileptic rats (right).

(D) Amplitude differences between groups were maintained ( $p < 0.0005$  and  $p < 0.0001$ ; for ripple and SPWs, respectively; Table 1).

(E) Time-frequency analysis was performed to examine the temporal dynamics of ripples and fast ripples. Note that ripple-frequency components were stable over the temporal course of the SPWs (left). Fast ripples emerged in the epileptic hippocampus from ripple oscillations as a second harmonic (right). Thick lines represent the normalized power spectra of these representative slices. Note the clear bimodal distribution in the epileptic case. The fast-ripple frequency band is marked by discontinuous lines.

(F) Correlation between the peak frequency of ripples and fast ripples ( $r = 0.89$ ,  $p < 0.0001$ ). Data from 53 hippocampal slices obtained from 30 epileptic animals.

(G) The fast ripple/ripple ratio is significantly different in control versus epileptic group ( $p < 0.0001$ ).

Error bars indicate the standard deviation.

a single episode of *status epilepticus* induced by i.p. injection of pilocarpine. Control groups included rats injected with saline ( $n = 10$ ) and those animals that were resistant to pilocarpine and did not exhibit *status* ( $n = 15$ ). Normal rats sharing similar housing conditions to these groups were also included as control ( $n = 20$ ). There were no significant differences between control groups. In particular, there were no differences in parameters obtained from pilocarpine-resistant rats compared with normal and saline-treated rats ( $p > 0.183$ ), and therefore data were pooled.

### Ripples and Fast Ripples in the Epileptic Hippocampus

Using bath solutions that physiologically increase excitability, we successfully induced spontaneous SPW ripples in conventional hippocampal slices prepared from these animals (see Experimental Procedures). Simultaneous field recordings from the stratum pyramidale of CA3 and CA1 regions revealed that these events were initiated in the CA3 area (Figure 1A). In control slices, SPW ripples consisted of a sharp transient potential associated with high-frequency oscillations of 100–300 Hz, but exhibiting nearly regular amplitude, in contrast with the irregular pattern seen in vivo (Buzsaki et al., 1983; Buzsaki and Chrobak, 2005). SPWs were also recorded in slices prepared from epileptic rats (Figure 1A, right). However, in these slices, very high frequency oscillations in the band of 200–600 Hz were detected in CA3 recordings, similar to fast ripples described in vivo (Bragin et al., 2002). The amplitude of SPW ripples was smaller in the epileptic group (Figure 1B).

Consistent with a local origin of these events in the highly recurrent CA3 network (Csicsvari et al., 2000), SPW ripples were recorded in the isolated CA3 region (Figure 1C; Experimental Procedures). Amplitude differences between control and epileptic groups were maintained (Figure 1D, Table 1, and Figure S1), as was the presence of fast ripples in the epileptic group. Time-frequency analysis suggested that fast ripples emerged from ripple oscillations as a second harmonic in the dynamical power spectrum (Figure 1E). Accordingly, the fast ripple peaked at  $523 \pm 64$  Hz, nearly doubling the ripple peak ( $269 \pm 37$  Hz) in all the slices examined ( $n = 53$  slices from epileptic rats). Strong correlation between ripple and fast ripple peak frequency confirmed that both processes were dynamically connected ( $r = 0.89$ ,  $p < 0.0001$ ; Figure 1F).

To quantitatively describe the frequency content of ripples and fast ripples, we constructed normalized power

**Table 1. Ripple and Fast Ripple Oscillations in the In Vitro Hippocampus**

	Control (40)	Epileptic (53)	t Test p Value
Ripple amplitude (mV)	$0.79 \pm 0.60$	$0.38 \pm 0.47$	0.0005
SPW amplitude (mV)	$1.69 \pm 0.77$	$0.92 \pm 0.66$	<0.0001
SPW duration (ms)	$55 \pm 8$	$56 \pm 9$	0.585
Normalized Power Spectrum: mean (Hz)	$362 \pm 27$	$389 \pm 22$	<0.0001
Normalized Power Spectrum: mode (Hz)	$277 \pm 38$	$267 \pm 37$	0.237
Normalized Power Spectrum: entropy (bits)	$4.93 \pm 0.11$	$5.09 \pm 0.08$	<0.0001
Fast ripple/ripple ratio	$0.49 \pm 0.14$	$0.69 \pm 0.15$	<0.0001

Numbers in parentheses indicate the number of slices. Data are given as mean  $\pm$  SD.

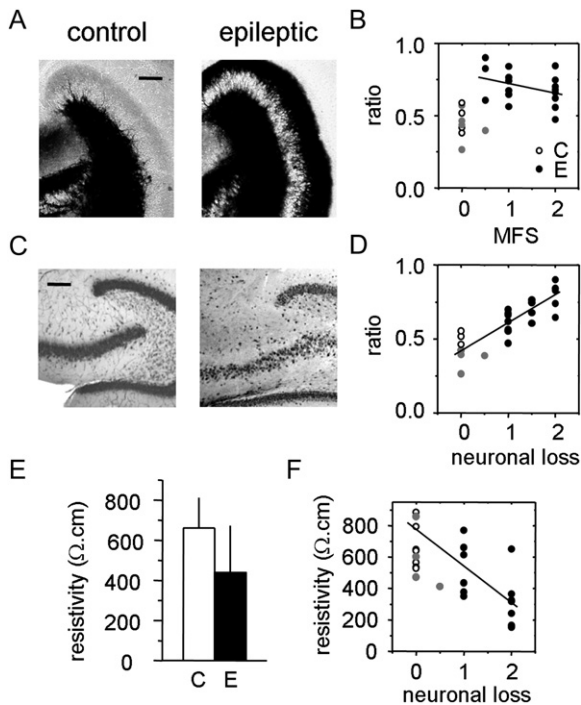


**Figure 2. Fast Ripples Correlate with Neuronal Cell Loss and Decreased Ephaptic Interactions in the Sclerotic Hippocampus**

(A) Timm staining was performed to evaluate mossy fiber sprouting (MFS) in slices from control (left) and epileptic animals (right). MFS was scored by two independent researchers to obtain mean values per slice and animal. Grade 0, no signs of MFS; grade 1, patchy staining of the supragranular layer; grade 2, dense continuous staining of the supragranular layer. Scale bar, 200  $\mu$ m.

(B) Absence of correlation between the MFS degree and the fast ripple/ripple ratio in epileptic rats ( $p = 0.1588$ ,  $n = 17$  rats). Data from nine control rats are given for comparison. Gray dots are data from pilocarpine-resistant control animals.

(C) NeuN immunostaining was used to evaluate neuronal loss in the CA3 region of control (left) and epileptic (right) animals. Neuronal loss was scored by two researchers according to three grades. Grade 0, no apparent neuronal loss; grade 1, patchy CA3c stratum pyramidale; grade 2, massive loss with severe interruption of the stratum pyramidale. Scale bar, 150  $\mu$ m.

(D) Positive correlation between neuronal loss and the fast ripple/ripple ratio ( $r = 0.86$ ,  $p < 0.0001$ ). Data from 17 epileptic and 9 control rats. Gray dots are data from pilocarpine-resistant control animals.

(E) Tissue resistivity was estimated to evaluate field interactions in the stratum pyramidale of normal and epileptic rats. We found lower tissue resistivity in epileptic animals compared with control ( $p = 0.0081$ ,  $n = 13$  slices from 7 epileptic rats;  $n = 11$  slices from 7 normal rats).

(F) Negative correlation between neuronal loss and tissue resistivity ( $r = -0.66$ ,  $p < 0.0005$ ) suggests lower field interactions in the sclerotic hippocampus. Gray dots are data from pilocarpine-resistant control animals.

Error bars indicate the standard deviation.

spectra and treated them as probability distributions (Experimental Procedures). The fast-ripple peak shifted the spectrum mean toward higher frequencies in the epileptic group (Figure 1E, thick line; Table 1). Consequently, the ratio between fast ripple and ripple power was significantly

higher in epileptic conditions ( $p < 0.0001$ ; Figure 1G). This disorganization of the oscillatory activity during SPW significantly increased the spectrum entropy in epileptic rats ( $p < 0.0001$ ; Table 1). In contrast, the spectrum mode, which captured the ripple peak frequency, was similar in both groups ( $p = 0.237$ ; Table 1 and Figure S1).

Overall, these findings suggest that fast ripples result from firing activity occurring out of the ripple phase. One possibility is that massive neuronal loss at the CA3 region of the sclerotic hippocampus may affect firing coordination due to lower field interactions (Snow and Dudek, 1986). Another possibility is that CA3 cells from the epileptic hippocampus fire at higher frequencies, giving rise to faster field oscillations. Additionally, since CA3 ripples result from organized neuronal firing in a highly recurrent network (Csicsvari et al., 2000), any process that impairs spike-timing reliability would affect ripple activity. We further explored these several, not mutually exclusive, possibilities at single-cell and circuit levels.

#### Fast Ripples Correlate with Neuronal Loss in the Sclerotic Hippocampus

Previous data suggest that fast ripples are associated with areas generating spontaneous seizures and exhibiting signs of hippocampal sclerosis (Bragin et al., 2002). Hippocampal sclerosis, the pathological hallmark of temporal lobe epilepsy, is characterized by mossy fiber sprouting and substantial cell loss in the hilus, portions of the CA3 and CA1 regions, and the entorhinal cortex (Babb and Brown, 1987). To further examine the relationship between fast ripples and hippocampal sclerosis, we correlated indices of mossy fiber sprouting and neuronal loss with fast-ripple power recorded in adjacent slices (see Experimental Procedures).

Hippocampi from epileptic rats exhibited clear signs of mossy fiber sprouting with different degrees, as scored using Timm staining and NPY immunohistochemistry (Experimental Procedures; Figure 2A). This ranged from a patchy staining of the supragranular layer (grade 1) to a dense continuous band (grade 2), in contrast to control rats that exhibited no signs of sprouting (grade 0). No correlation between the degree of mossy fiber sprouting and fast ripples was revealed in the epileptic group ( $p = 0.1588$ ; Figure 2B). However, a different picture emerged when fast-ripple power was compared with neuronal loss evaluated with NeuN immunohistochemistry (Figure 2C). In some rats, there was substantial cell death in CA3, which resulted in a blurry pyramidal layer (grade 2), whereas patchy strata were apparent in other cases (grade 1). We found a strong correlation between the expression of fast ripples and the degree of neuronal loss in the pyramidal layer of the CA3 region ( $r = 0.86$ ,  $p < 0.0001$ ; Figure 2D).

#### Neuronal Loss Results in Reduced Ephaptic Interaction

Field effects, or ephaptic interactions, facilitate synchronization in the hippocampus and are proposed to play a role

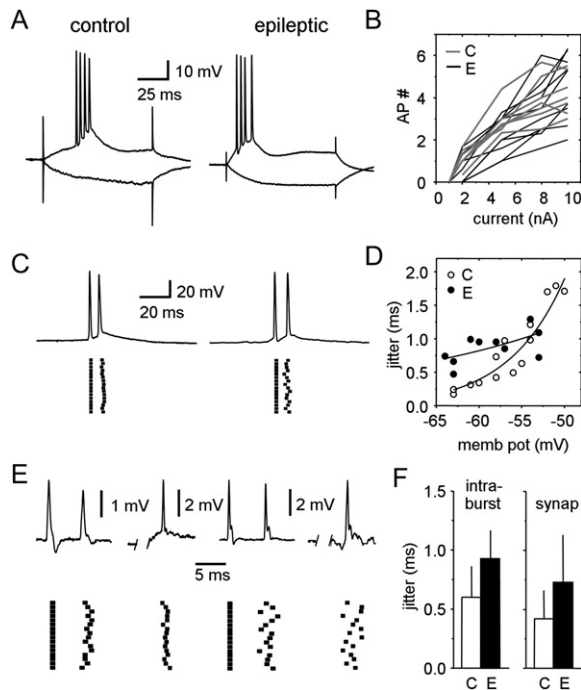


**Figure 3. Spike-Timing Reliability of CA3 Cells in Control versus Epileptic Animals**

(A) Intracellular recordings. Depolarizing and hyperpolarizing current pulses were used to characterize cell electrophysiology. CA3 cells typically discharge bursts of two to six action potentials.

(B) Input-output curves were similar in both groups ( $n = 7$  epileptic,  $n = 9$  control).

(C) Spontaneous bursts of two action potentials (doublets) were examined to uncover difference of spike-timing reliability. Note variability of the interspike interval (ISI) scatter plot of doublets recorded from CA3 cells in the epileptic hippocampus versus control.

(D) Plot of the intraburst jitter as a function of membrane potential in seven and five cells from control and epileptic rats, respectively.

(E) Juxtacellular recordings from CA3 pyramidal cells show variability of intraburst ISI (left) and synaptic responses (right) in control and epileptic rats. Artifacts of extracellular stimulation are blanked.

(F) (Left) Summary of intraburst jitter data from 15 (control) and 13 (epileptic) cells recorded juxtacellularly. (Right) Summary of synaptic jitter data from 8 (control) and 9 (epileptic) cells recorded juxtacellularly. Error bars indicate the standard deviation.

in firing coordination at high frequencies (Snow and Dudek, 1986; see Jefferys, 1995, for review). Increases of the extracellular space due to substantial cell loss would significantly decrease ephaptic interaction and eventually impair field oscillations. To explore this possibility, we chose to measure the tissue resistivity at the stratum pyramidale as an index of the efficacy of field effects in neuronal synchronization (Clark and Plonsey, 1970).

We found a lower tissue resistivity at the CA3 stratum pyramidale of epileptic rats compared with control ( $p = 0.0081$ ; Figure 2E). Moreover, resistivity was negatively correlated with the degree of neuronal loss observed in adjacent slices ( $r = -0.66$ ,  $p < 0.0005$ ; Figure 2F). Because the size of transmembrane potentials is directly proportional to extracellular resistivity (Clark and Plonsey,

1970), this supports the hypothesis of decreased ephaptic interactions in the sclerotic hippocampus. Indeed, we calculated the transmembrane potentials during SPW ripples (Snow and Dudek, 1986; see Experimental Procedures) and found lower values in epileptic ( $0.311 \pm 0.134$  mV,  $n = 6$ ) versus control cells ( $0.679 \pm 0.203$ ,  $n = 5$ ;  $p = 0.0027$ ). Therefore, in the sclerotic hippocampus, smaller field effects may act to impair firing coordination during SPW activity.

### Intrinsic Properties of CA3 Pyramidal Cells in Control versus Epileptic Animals

Recent data suggest that different kinds of channelopathies affect cellular excitability in temporal lobe epilepsy (Chen et al., 2001; Shah et al., 2004). One possibility is that altered cellular excitability in the epileptic hippocampus may be responsible for a higher-frequency component of ripple oscillations. We tested this possibility using intracellular recordings of CA3 pyramidal cells.

CA3 pyramidal cells discharge bursts of two to six action potentials (Wong and Prince, 1981). Input-output curves were obtained from intracellular records of pyramidal neurons from both groups (Figure 3A). There was no difference in the number of spikes evoked by the injection of depolarizing current pulses at similar membrane potentials (Figure 3B). Furthermore, the intraburst firing frequency was similar in both groups (Table 2), suggesting that fast ripples are not explained by higher-frequency firing of individual cells.

CA3 pyramidal neurons from epileptic rats exhibited similar mean resting membrane potentials but larger membrane potential fluctuations than did control neurons ( $p = 0.0077$ ; Table 2). Input resistance and membrane time constant were smaller in neurons from epileptic rats compared to control ( $p = 0.0067$  and  $p = 0.011$ , respectively; Table 2). Increased fluctuations seemed to result from enhanced synaptic activity, previously described in the epileptic hippocampus (Esclapez et al., 1999) (Figure S2). Accordingly, membrane potential fluctuations were significantly reduced by suppressing glutamatergic and GABAergic synaptic transmission, and differences between both groups were eliminated (Figure S2 and Table 2). Differences of input resistance and time constant between the epileptic and control groups were also abolished under these conditions (Table 2). Thus, although input-output responses to current injections were similar, larger membrane potential fluctuations due to an excessive synaptic activity in the epileptic hippocampus may critically affect neuronal dynamics during SPW events.

### Unreliable Spike Timing of CA3 Pyramidal Cells of the Epileptic Hippocampus

Intrinsic bursts from CA3 pyramidal cells depend on the membrane potential (Wong and Prince, 1981). We reasoned that large membrane potential fluctuations caused by excessive synaptic bombardment might result in unreliable bursting in the epileptic hippocampus. Additionally, synaptic responsiveness under these conditions would

**Table 2. Intrinsic Properties of CA3 Pyramidal Cells**

	Control (10)	Epileptic (9)	t Test p Value
Intraburst frequency (Hz)	239 ± 49	229 ± 51	0.669
Resting membrane potential (mV)	−60 ± 3	−57 ± 4	0.191
Membrane potential fluctuations (mV)	2.8 ± 1.2	4.1 ± 0.6	0.0077
Input resistance (MΩ)	26 ± 3	22 ± 2	0.0067
Membrane time constant (ms)	17.9 ± 3.3	14.1 ± 2.5	0.011
Doublets: intraburst ISI (ms)	5.05 ± 1.01*	5.06 ± 1.09*	0.989
Doublets: intraburst jitter (ms)	0.56 ± 0.29*	0.91 ± 0.24*	0.048
Synaptic Transmission Blocked			
	Control (6)	Epileptic (5)	t Test p value
Resting membrane potential (mV)	−66 ± 4	−62 ± 4	0.063
Membrane potential fluctuations (mV)	1.5 ± 0.2	1.7 ± 0.1	0.083
Input resistance (MΩ)	31 ± 8	32 ± 4	0.285
Membrane time constant (ms)	28.3 ± 2.1	25.3 ± 4.6	0.172

Numbers in parentheses indicate the number of cells. Data are given as mean ± SD. \*Data corresponds to n = 7 CA3 cells from control and n = 5 cells from epileptic animals.

be markedly affected. Because CA3 ripples result from coordinated neuronal firing (Csicsvari et al., 2000), unreliable spike timing could impair ripples. We explored indices of spike-timing reliability using intracellular and juxtacellular recordings of CA3 pyramidal cells.

At resting membrane potential, spontaneous bursts occurred between two consecutive SPWs and typically consisted of two (doublets) to three spikes. We noted that the intraburst frequency was more variable in CA3 pyramidal cells recorded from the epileptic hippocampus compared to controls (Figure 3C). We measured the intraburst jitter of doublets using at least two different membrane potentials in a group of cells. In neurons from control animals (n = 7), the intraburst jitter decreased with hyperpolarization, i.e., bursting became more regular as membrane potential hyperpolarized within a range (Wong and Prince, 1981) (Figure 3D). CA3 bursts from the epileptic hippocampus followed a similar relationship (n = 5 cells), but the jitter decreased less dramatically with hyperpolarization, and bursting was rare at membrane potentials positive to −50 mV (Figure 3D). At similar membrane potentials (−59 ± 2 mV), the intraburst jitter was significantly larger in neurons from the epileptic group compared to controls (p = 0.048; Table 2). No difference in the intraburst interspike interval (ISI) could explain this effect (p = 0.989; Table 2). Instead, the intraburst jitter was tightly correlated with membrane potential fluctuations (r = 0.72, p = 0.0083; Figure S3).

We checked for differences in the indices of spike-timing reliability between the two groups by using juxtacellular recordings, which noninvasively monitored the firing of individual cells (n = 15 control, n = 13 epileptic). We identified pyramidal cells using standard parameters of spike duration and burstiness (Ranck, 1973; Fox and Ranck,

1981). Cells recorded juxtacellularly fired doublets of similar intraburst ISI (p = 0.16) and intraburst jitter values (p = 0.59) compared to those previously observed intracellularly. Consequently, difference in intraburst jitter between control and epileptic groups was confirmed with noninvasive juxtacellular recordings (p = 0.0065; Figure 3F). We also evaluated whether spike-timing reliability of synaptic responses was impaired in the epileptic hippocampus. To this purpose, we applied mild extracellular stimulation in the vicinity of the recorded cells and measured the jitter in the latency of synaptic responses (Figure 3E). We observed a significantly larger jitter in epileptic (n = 9) versus control cells (n = 8, p = 0.047; Figure 3F). No difference in the mean latency could explain this variation (3.71 ± 0.71 and 3.26 ± 0.78, p = 0.26, for epileptic and control, respectively).

#### Unreliable Spike Timing Is Associated with the Generation of Fast Ripples

Our data indicate that spike-timing reliability is reduced in CA3 cells from epileptic rats. This, together with lower efficacy of field interactions, might result in reduced neuronal synchronization and distortion of the ripple pattern. In order to link these two levels, we examined the firing dynamics of single cells during SPW ripples using combined juxtacellular and nearby field potential recordings.

We analyzed juxtacellular recordings from 36 CA3 pyramidal cells from both epileptic and control animals. In control animals, cells displayed different but unique firing patterns during SPW ripples (n = 11 cells). Some neurons fired all along the SPW, whereas others tended to discharge only during specific portions of the event or were even silenced (Figure S4). However, in spite of this cell-to-cell variability, we found a precise temporal relationship

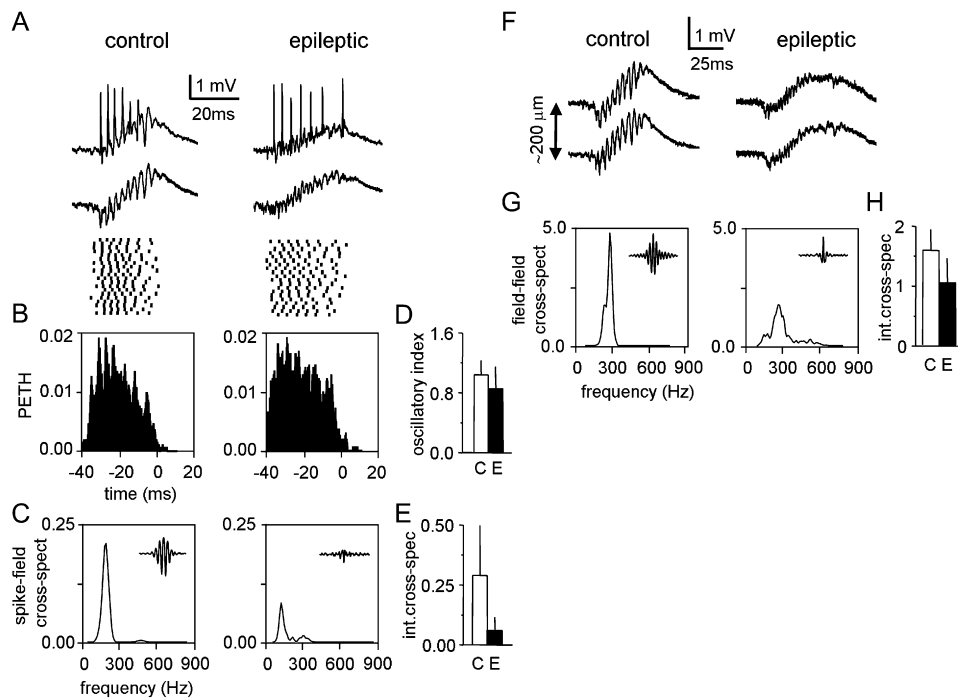


**Figure 4. Single-Cell Firing Dynamics during Ripples and Fast Ripples**

(A) Simultaneous juxtacellular and field recordings were obtained to evaluate firing dynamics during ripples and fast ripples in CA3 slices from control (left) and epileptic rats (right). Scatter plot representation of neuronal firing highlights unreliable cell firing in representative cases from the epileptic (right) versus control group (left).

(B) Peri-event time histograms (PETH) reflect differences of the SPW-associated neuronal firing in control versus epileptic. PETHs from cells shown in (A).

(C) Spike-field cross-spectra in representative slices for the control (left) and epileptic animals (right). Note that, in spite of a weaker correlation between single-cell firing and the field in the epileptic case, the spectrum peak remained in the ripple band. The insets represent the corresponding spike-field cross-correlation function.

(D) Summary of the oscillatory index of PETH data from 11 (control) and 25 cells (epileptic). Significantly different at  $p = 0.035$ .

(E) Summary of the spike-field synchronization data measured as the integral of the spike-field cross-spectra. Significantly different at  $p = 0.0084$ .

(F) Simultaneous field recordings separated 100–200  $\mu\text{m}$  in representative slices from control (left) and epileptic animals (right).

(G) Field-field cross-spectra from recordings in (F) showing the loss of spatial synchronization in the epileptic case (right) compared to control (left). The insets represent the corresponding field-field cross-correlations.

(H) Summary of spatial synchronization data measured as the integral of the field-field cross-spectrum from 12 (control) and 25 slices (epileptic; significantly different,  $p = 0.0084$ ).

Error bars indicate the standard deviation.

between single-cell firing and the SPW peak across successive events (Figure 4A, left). Peri-event time histograms (PETH) from control cells reflected a clear oscillatory pattern (Figure 4B, left). ISI histograms of individual cells during SPWs showed that cells fired within the ripple frequency band ( $279 \pm 57$  Hz). By computing the spike-field cross-spectrum using spike-triggered averages of several consecutive events (Experimental Procedures), we found that individual cell firing was tightly correlated with ripple oscillation in the nearby field (Figure 4C, left). As expected, the peak of the spike-field cross-spectrum ( $286 \pm 56$  Hz) was almost at the same frequency as the ripple peak in the nearby field ( $288 \pm 63$  Hz). Indeed, the cross-spectrum between fields separated 100–200  $\mu\text{m}$  (Figure 4F, left) also indicated large spatial synchronization within the ripple frequency band ( $n = 12$  slices; Figure 4G, left).

In contrast, PETH from the epileptic group did not display a clear oscillatory pattern across several SPW fast ripple events ( $n = 25$  cells; Figure 4B, right). An oscillatory index defined from the PETH (Experimental Procedures) was smaller in the epileptic group, indicating unstructured firing ( $p = 0.035$ , one-tail; Figure 4D). The PETH oscillatory index did not correlate with SWP amplitude ( $r = -0.13$ ,  $p = 0.45$ ), suggesting that the disorganization of the PETH could not be explained by poor triggering of SPW events due to their smaller amplitude in the epileptic group. Indeed, the weaker correlation between single-cell firing and the field event in the epileptic group was confirmed by the spike-field cross-spectrum (Figure 4C, right) yielding smaller values of the integral ( $p = 0.0084$ ; Figure 4E), which is a measure of the overall spike-field synchronization. However, the cross-spectrum peak was still within the ripple frequency band ( $275 \pm 74$  Hz; Figure 4C, right),

in spite of the higher fast-ripple component in the nearby field. The ISI histogram of CA3 cells from the epileptic hippocampus confirmed that they exclusively fired within the ripple band ( $269 \pm 48$  Hz) and that they did not follow fast-ripple frequencies. The cross-spectrum between fields (Figures 4F and 4G, right) showed a weaker spatial synchronization in the epileptic group ( $n = 25$  slices; Figure 4H). Nonetheless, spatial synchronization preferentially remained within the ripple frequency band despite the presence of fast ripples (Figure 4G, right).

### Improved Spike-Timing Reliability Is Associated with the Restoration of Ripples in the Epileptic Hippocampus

Altogether, our data suggest that firing coordination is disrupted in the epileptic hippocampus, resulting in shuffled ripple oscillations that generate fast ripples. Accordingly, unreliable spike timing at the cellular level might result in dissimilar firing dynamics and temporal and spatial disorganization of ripple patterns at the population level. Therefore, manipulations that improve spike-timing reliability should be successful in restoring ripple oscillations in the epileptic hippocampus.

As previously noted, large membrane potential fluctuations caused by intense synaptic bombardment were responsible for the loss of spike-timing reliability in cells from the epileptic hippocampus. We therefore chose to apply low concentrations of NBQX ( $1\text{--}1.5 \mu\text{M}$ ) after blocking GABAergic neurotransmission (Figure S5) to reduce synaptic activity and increase spike-timing reliability in the epileptic hippocampus (Figure 5A). This strategy successfully reduced the intraburst jitter in 4 of 4 cells ( $p = 0.033$ , paired; Figure 5B) and increased spatial synchronization of fields separated by  $100\text{--}200 \mu\text{m}$  ( $p = 0.035$ , paired,  $n = 9$  slices; Figures 5C and 5D). As a result, the ripple pattern was restored at the population level (Figure 5E) and field oscillations reorganized ( $p = 0.0024$ , paired,  $n = 15$  slices; Figure 5F).

Spike-timing reliability of synaptic responses is mainly dominated by disinaptic inhibition mediated by GABA<sub>A</sub> receptors (Pouille and Scanziani, 2001). Hence, we used diazepam ( $4 \mu\text{M}$ ) to enhance fast GABAergic inhibition and to reduce unreliable synaptic responses in the epileptic hippocampus ( $p = 0.039$ , paired, 5/5 cells; Figures 5G and 5H). Diazepam did not affect the intraburst jitter in 4 out of 9 cells ( $p = 0.27$ , paired), whereas the remaining 5 neurons were silenced between SPWs. Applying diazepam resulted in increased spatial synchronization of field activity within the ripple frequency band ( $p = 0.018$ ,  $n = 7$  slices; Figures 5I and 5J). Consequently, fast ripples were reduced, and ripples were restored ( $p = 0.0032$ , paired,  $n = 15$  slices; Figures 5K and 5L).

### Reduced Spike-Timing Reliability Correlates with Ripple Shuffling in the Normal Hippocampus

Finally, we looked for evidence of the impact of spike-timing reliability on ripple oscillations in the absence of neuronal loss. We reasoned that if reduced firing precision of in-

dividual cells is a critical condition for the emergence of fast ripples, we should be able to deteriorate ripples by interfering with mechanisms regulating neuronal firing in the normal hippocampus. We choose to reduce firing reliability in the control hippocampus by using tetraethylammonium (TEA), a blocker of the delayed rectifier potassium current (Storm, 1990). At concentrations of  $0.8\text{--}1$  mM, TEA induced a near 2-fold increase of both the intraburst ISI and jitter of pyramidal cells from the normal hippocampus (Figures 6A and 6B;  $n = 6$  cells) (Klee et al., 1995). At the population level, the spatial synchronization of fields separated by  $200 \mu\text{m}$  was significantly reduced ( $p = 0.0272$ , paired,  $n = 9$  slices; Figures 6C and 6D) and ripple oscillations deteriorated (Figure 6E). Time-frequency analysis revealed the emergence of a second harmonic component remarkably similar to the fast ripples that we observed in epileptic slices, which resulted in increased spectrum entropy ( $p = 0.0162$ , paired,  $n = 9$  slices; Figure 6F).

## DISCUSSION

We have examined the mechanisms of ripples and fast ripples in the CA3 hippocampal region using an *in vitro* model of sharp waves. Our data suggest that fast ripples reflect desynchronized rather than hypersynchronized activity in the isolated CA3 region of the sclerotic hippocampus. Fast ripples dynamically emerge from a disorganization of the ripple pattern, which is associated with unreliable firing of CA3 cells due to large synaptically driven membrane potential fluctuations. A weaker synchronization between individual cell firing and circuit oscillations correlates with ripple shuffling and the emergence of fast ripples. Reducing membrane potential fluctuations improves both spike-timing reliability and spatial synchronization and restores ripple oscillations in the epileptic hippocampus. On the contrary, reducing spike-timing reliability in the normal hippocampus, by interfering with the delayed rectifier potassium current, correlates with deterioration of ripples. Altogether, our data support the idea that reduced spike-timing reliability is associated with the emergence of fast ripples in the epileptic hippocampus.

The cellular and network mechanisms of ripples are still under debate. The SPW ripples arise from the highly recurrent CA3 region and spread downstream as a spatially coherent oscillation all along the CA1-subicular-entorhinal axis (Chrobak and Buzsaki, 1996). Discharges of CA3 cells converge onto both CA1 pyramidal cells and interneurons through the Schaffer collateral system and temporarily reset their firing (Ylinen et al., 1995; Somogyi and Klausberger, 2005). In CA1, ripples are detected at the stratum pyramidale in tandem with the SPW potential at the stratum radiatum (Ylinen et al., 1995), and they are thought to reflect synchronous firing of pyramidal cells and interneurons differentially coupled to each oscillatory cycle (Csicsvari et al., 1999, 2000). Both synaptic and electrical interactions may assist in this synchronization process (Draguhn et al., 1998; Traub and Bibbig, 2000; Dzhala

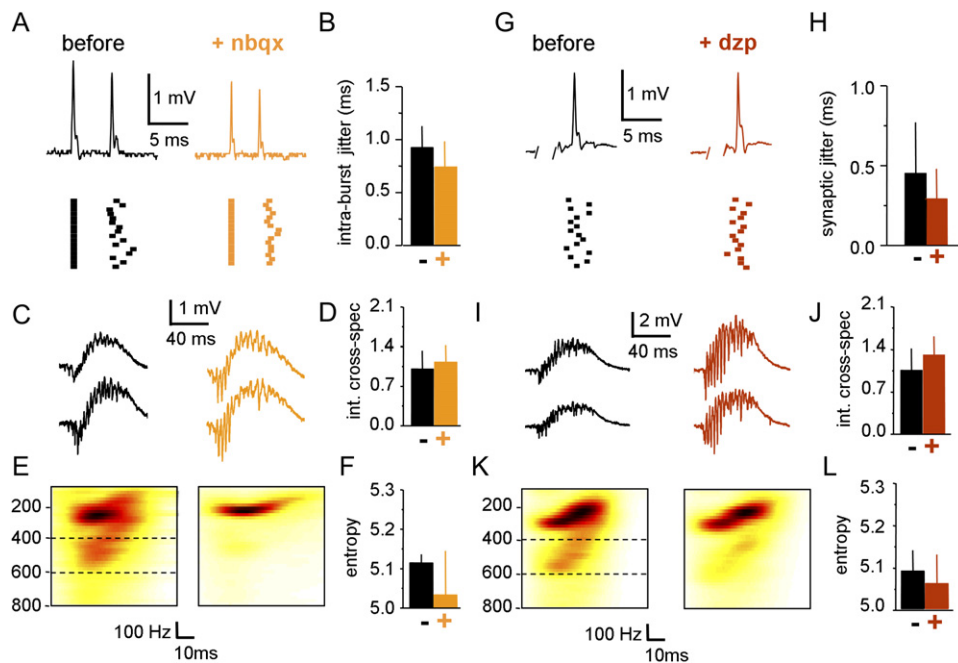


**Figure 5. Improving Spike-Timing Reliability Restores Ripples in Slices from Epileptic Animals**

(A) Applying low concentrations of NBQX (1–1.5  $\mu$ M) resulted in reduction of the intraburst jitter in juxtacellular recordings.

(B) Summary of the intraburst jitter data ( $p = 0.033$ , paired,  $n = 4$  cells).

(C) Low concentrations of NBQX increased spatial synchronization in field recordings separated by 100–200  $\mu$ m.

(D) Summary of spatial synchronization data from nine slices ( $p = 0.035$ , paired).

(E) Time-frequency analysis showed that fast ripples were reduced and ripples were restored in the epileptic hippocampus after application of low concentrations of NBQX.

(F) Summary of time-frequency data showing the reduction of the entropy of the power spectrum distribution after NBQX ( $p = 0.0024$ , paired,  $n = 15$  slices).

(G) Applying diazepam (4  $\mu$ M) resulted in reduction of synaptic jitter in juxtacellular recordings.

(H) Summary of the synaptic jitter data ( $p = 0.039$ , paired,  $n = 5$  cells).

(I) Diazepam increased spatial synchronization in field recordings separated 100–200  $\mu$ m.

(J) Summary of spatial synchronization data from seven slices ( $p = 0.018$ , paired).

(K) Time-frequency analysis showed that fast ripples were reduced and ripples were restored in the epileptic hippocampus after application of diazepam.

(L) Summary of time-frequency data showing the reduction of the entropy of the power spectrum distribution after diazepam ( $p = 0.0032$ , paired,  $n = 15$  slices).

Error bars indicate the standard deviation.

and Staley, 2004). One of the first ideas to explain CA1 ripples was proposed from the observation that fast IPSPs converging on pyramidal cells were coupled to ripple oscillation (Ylinen et al., 1995). However, axo-axonic and oriens-alveus interneurons are silenced during SPWs, whereas basket cells and bistratified interneurons increase their firing with different temporal dynamics (for review, see Somogyi and Klausberger, 2005). Therefore, interneurons belonging to different classes follow different firing dynamics during a given SPW event. In contrast, summed activity of CA1 pyramidal cells recorded in parallel seems to be better predictor of ripples than the firing of some populations of interneurons (Csicsvari et al., 1999, 2000).

Ripples in the CA3 region in vivo are slower (50–120 Hz), and their mechanisms are even less well understood (Ylinen et al., 1995; Buzsaki and Chrobak, 2005). Our in vitro

data support the idea that CA3 ripples mainly result from the coordinated burst of a group of pyramidal cells sharing similar firing properties (Dzhala and Staley, 2004). Pyramidal cells displayed different but stereotyped firing patterns that successfully match field oscillations. Intracellularly, complex but unique sequences of excitation and inhibition indicate that, in spite of a cell-to-cell variability, firing sequences across different cell assemblies are imprinted in the network and dominate single-cell dynamics (Mendez de la Prida and Gal, 2004; Behrens et al., 2005). Consequently, CA3 cell firing during SPW ripples in vitro is coordinated synaptically with the intrinsic cellular dynamics shaping the field oscillation (Draguhn et al., 1998; Dzhala and Staley, 2004; Behrens et al., 2005). Yet, the in vitro SPW-ripple pattern is not identical to that observed in vivo (Buzsaki and Chrobak, 2005). First, CA3 ripples in vivo are very irregular in both their temporal and amplitude

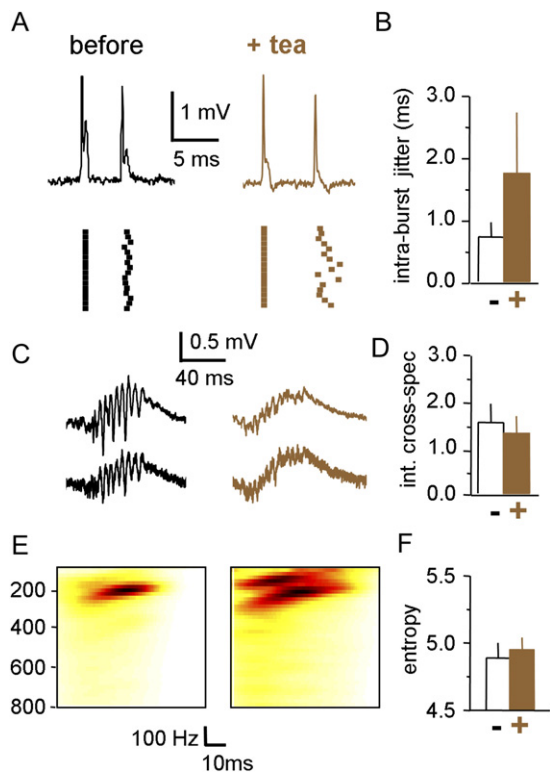


**Figure 6. Reducing Spike-Timing Reliability Deteriorates Ripples in the Normal Hippocampus**

(A) Applying tetraethylammonium (TEA) at 0.8–1 mM resulted in increased intraburst jitter in juxtacellular recordings.

(B) Summary of the intraburst jitter data ( $p = 0.0134$ , paired,  $n = 6$  cells).

(C) TEA at 0.8–1 mM decreased spatial synchronization in field recordings separated by 100–200  $\mu\text{m}$ .

(D) Summary of spatial synchronization data ( $p = 0.0272$ , paired,  $n = 9$  slices).

(E) Time-frequency analysis showed that ripples were deteriorated and their period doubled after application of TEA.

(F) Summary of time-frequency data showing the increase of the entropy of the power spectrum distribution after TEA ( $p = 0.0162$ , paired,  $n = 9$  slices).

Error bars indicate the standard deviation.

distribution, in contrast to the uniformly sized and well-organized SPW ripples in vitro (Ylinen et al., 1995). Second, pyramidal cell firing in vivo exhibits substantially more variability: some neurons discharge in successive events, whereas others fire very rarely (Buzsaki et al., 1992; Csicsvari et al., 1999; Somogyi and Klausberger, 2005).

However, in spite of these differences, several pieces of evidence suggest that similar mechanisms can operate in both conditions. CA3 pyramidal cells in vivo burst intrinsically when disinhibited due to the behavioral-dependent reduction of neuromodulator release during immobility and slow-wave sleep (Thompson et al., 1993). Recent in vivo data indicate that more than 10% of CA3 pyramidal cells discharge synchronously within a short time window to produce detectable SPWs at the CA1 area (Csicsvari

et al., 2000). Therefore, both in vivo and in vitro, the emergent population burst in the CA3 region is brought about by the recurrent collateral system acting to locally synchronize cell assemblies (Buzsaki and Chrobak, 2005; Menendez de la Prida et al., 2006). This view does not exclude a possible implication of coordinated interneuron firing in ripples nor that synaptic interactions between pyramidal cells and interneurons may also play a role (Ylinen et al., 1995; Csicsvari et al., 1999). Also, other factors, including neurotransmitter release and gap junction transmission, may be involved (Staley et al., 1998; Draguhn et al., 1998). Indeed, anesthetics that reduce transmitter release have proven to significantly decrease the frequency of ripple oscillations in vivo (Ylinen et al., 1995). However, our data suggest that spike-timing reliability of CA3 pyramidal cells is related with the emergence of ripples, because manipulations that interfere with firing precision modulate the ripple oscillatory pattern.

We recorded fast ripples at the CA3 area of the hippocampus from lithium-pilocarpine-treated rats. There was a close relationship between widespread neuronal loss and fast ripples, which together with their presence at regions generating seizures further supports the idea of fast ripples as markers of epileptogenic areas (Bragin et al., 2002; Jirsch et al., 2006). We found that CA3 pyramidal cells from the epileptic hippocampus exhibited larger synaptically driven membrane potential fluctuations than control cells. This condition is brought about by intense synaptic bombardment, probably resulting from local axonal reorganization following cell death in the CA3 sclerotic region (Nadler et al., 1980; Siddiqui and Joseph, 2005). Previous data pointed to a local reorganization of inhibitory and excitatory circuits in the epileptic hippocampus (Nadler et al., 1980; Siddiqui and Joseph, 2005; Kobayashi and Buckmaster, 2003; Shao and Dudek, 2005). As a result, sprouted glutamatergic terminals (Nadler et al., 1980; Siddiqui and Joseph, 2005), together with pre- and postsynaptic alterations in the GABAergic control, drive enhanced synaptic activity, which results in large membrane potential fluctuations (Esclapez et al., 1999; Hirsch et al., 1999). Under these conditions, individual cell firing during SPWs was weakly correlated at the population level, and ripple oscillation disorganized. We show that reducing synaptically driven membrane potential fluctuations increased spike-timing reliability and successfully restored ripples, even in the sclerotic hippocampus. Moreover, decreasing the spike-timing reliability in the normal hippocampus by interfering with the delayed rectifier potassium current (Klee et al., 1995) was associated with the emergence of fast ripples at the population level. Although these manipulations may also affect neurotransmitter release, spike duration, inhibitory cell function, etc., the combined experimental results are all consistent with a role of spike-timing reliability in the genesis of ripples and fast ripples.

Overall, we show that fast ripples in vitro emerge as a pathological desynchronization of the normal ripple pattern. Note that our data do not exclude the possibility that

clusters of highly interconnected neurons were responsible for fast ripples (Bragin et al., 2000) but suggest that fast ripples do not represent hypersynchronous bursting (Bragin et al., 2000, 2002). Yet, cells in the epileptic hippocampus fired unreliably during SPWs, resulting in the impairment of the temporal and spatial firing coordination. However, single-cell firing and spatial synchronization of field oscillations still occurred preferentially at the ripple frequency band, suggesting that the higher-frequency component of fast ripples is not emerging at the cellular level and that the hippocampal circuitry is tuned to oscillate at the ripple band. This further suggests that fast ripples arise from the interaction between various ripple generators in neighboring sites. Notably, fast ripples were related harmonically with ripples, suggesting that these interactions should follow dynamical rules governing nonlinear systems (Feigenbaum, 1979). While future work is required to understand these rules, the present study establishes a relationship between reduced spike-timing reliability and the emergence of fast ripples in the epileptic hippocampus.

## EXPERIMENTAL PROCEDURES

### Lithium-Pilocarpine Treatment

Adult male Sprague-Dawley rats (180–200 g) were i.p. injected with pilocarpine hydrochloride 12–24 hr after injection of lithium (127 mg/kg, i.p.). Between one and four doses of 10 mg/kg pilocarpine were injected every 30 min until the *status epilepticus* was reached. Diazepam (4 mg/kg, i.p.) was injected 1 hr after the *status* and repeated if needed during the following 24 hr. Animals were i.p. injected with 2.5 ml 5% dextrose several times a day, and diet was supplemented with fruit and powder milk during the following 2–3 days. Saline controls were the same age group as drug-treated rats and received identical treatment (lithium and diazepam). Animals that did not exhibit *status* after four doses of 10 mg/kg pilocarpine were considered resistant. Rats were observed for spontaneous seizures at random times between 8 a.m. and 7 p.m. during at least 20 min and 2–3 times per week. When no spontaneous seizure was observed, animals were continuously tape recorded during 48–72 hr. Spontaneous seizures were scored according to Racine (Racine, 1972). All procedures concerning animals met the European guidelines (86/609/EEC).

### In Vitro Electrophysiology

Rats were anesthetized with ether, and the brain was immediately removed and chilled in 4°C oxygenated (95% O<sub>2</sub>/5% CO<sub>2</sub>) artificial cerebrospinal fluid (ACSF: 125 mM NaCl, 4 mM KCl, 1 mM MgCl<sub>2</sub>, 1.2 mM NaH<sub>2</sub>PO<sub>4</sub>, 1 mM CaCl<sub>2</sub>, 22 mM NaHCO<sub>3</sub>, 10 mM glucose). Horizontal slices (350 μm) were prepared from the mid-septotemporal level of the hippocampus. Minislices containing the CA3c region were prepared using dissection scissors (Figure S6). Slices were maintained in ACSF at room temperature for at least 2 hr before being transferred to an interface recording chamber at 32°C–34°C.

Spontaneous SPW-ripple events were induced by reducing extracellular Ca<sup>2+</sup> concentration and increasing K<sup>+</sup> in a physiological range (Figure S7). We typically used 1 mM Mg<sup>2+</sup>, 1 mM Ca<sup>2+</sup>, and 4 mM K<sup>+</sup>. Extracellular field recordings were obtained using broken pipettes filled with ACSF (tip diameter ~10 μm, resistance ~4 MΩ). Pipettes were made from borosilicate glass capillaries (outer diameter 1.2 mm, inner diameter 0.69 mm; Harvard Apparatus). Field signals were preamplified using high-impedance FETs and band-pass filtered at 0.1 Hz to 3 KHz. 50–60 Hz noise was suppressed using Humbugs (Quest Scientific). Monopolar square-wave stimulation (0.1 ms dura-

tion) was delivered via tungsten electrodes. Tissue resistivity in the CA3c stratum pyramidale was estimated using double glass pipettes under visual control. Pulses of 50 ms and various amplitudes were injected into one barrel, and the voltage change was measured at the other barrel. The ratio between voltage drops obtained in the slice and in the perfusate of known resistivity (~60 Ω·cm; Clark and Plonsey, 1970) was used to estimate tissue resistivity (Lopez-Aguado et al., 2001). Intracellular sharp recordings from CA3 pyramidal cells were obtained using glass pipettes filled with 2 M K-acetate (tip resistance 60–80 MΩ) and an Axoclamp 2B amplifier (Axon Instruments). Only cells with stable membrane potentials negative to –55 mV, overshooting action potentials and input resistance >20 MΩ, were considered. Depolarizing and hyperpolarizing currents of 50 and 500 ms were used to characterize cell electrophysiology. To evaluate transmembrane potentials during SPW-ripple events in the epileptic versus control hippocampus, we obtained differential recordings between an intracellular electrode and an adjacent extracellular electrode in a group of cells (Snow and Dudek, 1986). Similar field fluctuations during SPW ripples in both electrodes were controlled before establishing the intracellular recordings. We calculated the transmembrane potential by subtracting the intracellular minus the adjacent field recording during different ripple cycles.

Juxtacellular recordings were obtained using patch pipettes filled with ACSF (tip resistance ~7 MΩ) driven by a piezoelectric manipulator that was advanced by 1–10 μm into the stratum pyramidale. In these experiments, another pipette filled with ACSF was located near the recorded cell (50–150 μm). All signals were digitized using a 12 bit, 16 channel A-D converter (Digidata 1200A, Axon Instruments) and were sampled at 20 kHz. All neurophysiological data were exported to MATLAB (v. 6.5, MathWorks) for further analysis.

### Histology and Immunohistochemistry

We systematically separated two to four slices per animal for posterior histological examination. All slices were immersion-fixed in cold phosphate-buffered (PBS) 4% paraformaldehyde. Standard procedures for Timm staining included a prefixation in cold 0.37% Na<sub>2</sub>S PBS to precipitate the zinc in the mossy fibers. The tissue was then sectioned at 70 μm (Timm) or 100 μm (immunostaining). For the Timm staining, free-floating sections were developed in the dark, using arabic gum, citric acid, hydroquinone, and silver nitrate during at least 1 hr. For immunostaining, free-floating sections were washed in 0.1 M PBS followed by incubation in 1% H<sub>2</sub>O<sub>2</sub> for 45 min. After washing in PBS several times, sections were maintained during 1 hr in PBS containing 10% fetal bovine serum (FBS) or normal goat serum (NGS) and 0.25% Triton. Sections were then incubated overnight at 4°C in antisera to NeuN (in mouse, 1:1000, Bachem) or NPY (in rabbit, 1:1000, Peninsula) diluted in PBS containing 1% FBS and 0.25% Triton. On the second day, sections were incubated for 2 hr in biotinylated anti-mouse or anti-rabbit (1:200; Vector). After washing, sections were incubated for 1 hr in avidin-biotin-horseradish peroxidase complex (1:1000, Vector) diluted in PBS. Sections were washed in PBS and developed in 0.05% diaminobenzidine tetrahydrochloride (Sigma). Sections were mounted on slides and coverslipped with Eukitt (Fluka). Mossy fiber sprouting and neuronal loss were scored by two independent researchers to obtain mean values per slice and animal. Adjacent slices for a given animal typically gave similar indices of mossy fiber sprouting and neuronal loss.

### Data Analysis

Field recordings were low-pass filtered at 100 Hz to study SPWs and band-pass filtered between 100 and 800 Hz to study ripples and fast ripples, using forward-backward zero-phase FIR filters of order 512. SPWs were automatically detected by thresholding and visually verified offline. The positive peak of each individual SPW was used as a trigger for subsequent field and spike-field analyses of SPW-associated ripple and fast-ripple oscillations. The instantaneous ripple amplitude was evaluated by applying the Hilbert transform to the 100–800

Hz filtered data. The SPW amplitude was calculated as the voltage difference of the positive peak of the averaged low-pass-filtered field recording. The SPW and ripple amplitude is reported as mean values per slice.

Time-frequency representations of the ripple dynamics were obtained for each slice by averaging the short-time fourier transform (STFT) of individual SPW-ripple events. STFTs were performed with mean detrending, Hanning windowing and FFT size of 1024 points with 1000 points overlap. The overall ripple spectrum was estimated by averaging the time-frequency representation over the time axis. In order to study the frequency content of ripple and fast ripples independently of amplitude changes, each spectrum was normalized by the power between 100 and 800 Hz. We therefore obtained power spectra with unitary area, which we treated as statistical distributions. We then extracted three main parameters: (1) the mean, which represents the average field oscillatory frequency, (2) the mode, which represents the peak frequency of field oscillations, and (3) the entropy, which is a measure of the frequency dispersion. The entropy (in bits) was calculated as

$$-\sum_f p(f) \cdot \log_2(p(f))$$

where  $p(f)$  is the 100–800 Hz normalized power spectrum and  $f$  denotes frequency. In recordings from the epileptic hippocampus, frequency distributions were bimodal due to the presence of fast ripples. In these cases, the main frequency of fast ripples was calculated as the mode of the second peak. We also integrated the normalized power spectrum within specific frequency ranges to calculate the normalized ripple power (100–300 Hz) and the normalized fast ripple power (400–600 Hz). The fast ripple/ripple ratio was evaluated as the ratio between the above two measures. Note that the fast ripple/ripple ratio does not depend on the normalization of the spectrum.

In juxtacellular recordings, spikes were discriminated using standard threshold-based procedures of high-pass-filtered data (500 Hz). All spikes were visually checked to eliminate possible contamination. Interspike interval histograms were constructed using spikes fired during and between SPW-ripple events in each condition. The inverse of the ISI histogram peak was used as a measure of firing frequency of each cell. The intraburst jitter of spontaneous firing was defined as the standard deviation of the corresponding ISI histogram. Peri-event time histograms were triggered by the SPW peak from the nearby field recording. PETHs were obtained at 0.25 ms bin size and smoothed with a 5 points moving average. An oscillatory index was defined by high-pass filtering each PETH above 100 Hz and by calculating the decimal logarithm of the ratio, expressed as a percentage, between the variance of the high-filtered PETH and the variance of the original smoothed PETH.

Spike-field cross-spectra were evaluated by (1) concatenating SPW-ripple events, (2) calculating the cross-correlation function between the discriminated spikes and the nearby field recording, and (3) estimating the spectrum of the spike-field cross-correlation function. To keep spike-field cross-spectra independent of signal amplitude, the auto-correlation function of the spikes and the fields were normalized. Note that the spike-field cross-correlation function mathematically corresponds to the well-known spike-triggered average and does not depend on SPW triggering. The spectrum of the spike-triggered average was calculated with a FFT by applying one 2048 points Hanning window centered on lag zero, with mean detrending. The decimal logarithm of the integral of the spike-field cross-spectrum was used as a measure of the overall spike-field synchronization. Field-field cross-spectrum and field-field spatial synchronization were calculated in the same way, but substituting the spikes by another field recording.

All results are given as mean  $\pm$  SD. Results were compared using Student's *t* test at  $p = 0.05$ . Precise *p* values are indicated in every case, except when  $p < 0.0001$ . Simple linear regression was performed with a confidence interval of 95%.

### Supplemental Data

The Supplemental Data for this article can be found online at <http://www.neuron.org/cgi/content/full/55/6/930/DC1>.

### ACKNOWLEDGMENTS

We thank Richard Miles and Aric Agmon for comments on this manuscript. We also thank Oscar Herreras for discussion on the method for estimating tissue resistivity and for sharing recordings facilities with us; Helen Scharfman for useful suggestions on animal care after the *status epilepticus*; and Carlos Lopez-Garcia for helping us with the Timm protocol. Supported by grants from the Spanish Ministry of Education and Science (BFU2006-10584-BF) and Fondo de investigaciones Sanitarias de Castilla-La Mancha FISCAM (PI-2006/49).

Received: March 19, 2007

Revised: June 6, 2007

Accepted: July 31, 2007

Published: September 19, 2007

### REFERENCES

- Babb, T.L., and Brown, W.J. (1987). Pathological findings in epilepsy. In *Surgical Treatment of the Epilepsies*, J. Engel, Jr., ed. (New York: Raven Press), pp. 511–540.
- Behrens, C.J., van den Boom, L.P., de Hoz, L., Friedman, A., and Heinemann, U. (2005). Induction of sharp wave-ripple complexes in vitro and reorganization of hippocampal networks. *Nat. Neurosci.* 8, 1560–1567.
- Bragin, A., Engel, J., Jr., Wilson, C.L., Fried, I., and Mathern, G.W. (1999). Hippocampal and entorhinal cortex high-frequency oscillations (100–500 Hz) in human epileptic brain and in kainic acid-treated rats with chronic seizures. *Epilepsia* 40, 127–137.
- Bragin, A., Wilson, C.L., and Engel, J., Jr. (2000). Chronic epileptogenesis requires development of a network of pathologically interconnected neuron clusters: a hypothesis. *Epilepsia* 41 (Suppl 6), S144–S152.
- Bragin, A., Mody, I., Wilson, C.L., and Engel, J., Jr. (2002). Local generation of fast ripples in epileptic brain. *J. Neurosci.* 22, 2012–2021.
- Buzsaki, G., and Chrobak, J.J. (2005). Synaptic plasticity and self-organization in the hippocampus. *Nat. Neurosci.* 8, 1418–1420.
- Buzsaki, G., Leung, L.W., and Vanderwolf, C.H. (1983). Cellular bases of hippocampal EEG in the behaving rat. *Brain Res. Brain Res. Rev.* 287, 139–171.
- Buzsaki, G., Horvath, Z., Urioste, R., Hetke, J., and Wise, K. (1992). High-frequency network oscillation in the hippocampus. *Science* 256, 1025–1027.
- Chen, K., Aradi, I., Thon, N., Eghbal-Ahmadi, M., Baram, T.Z., and Soltesz, I. (2001). Persistently modified h-channels after complex febrile seizures convert the seizure-induced enhancement of inhibition to hyperexcitability. *Nat. Med.* 7, 331–337.
- Chrobak, J.J., and Buzsaki, G. (1996). High-frequency oscillations in the output networks of the hippocampal-entorhinal axis of the freely behaving rat. *J. Neurosci.* 16, 3056–3066.
- Clark, J.W., and Plonsey, R. (1970). A mathematical study of nerve fiber interaction. *Biophys. J.* 10, 937–957.
- Csicsvari, J., Hirase, H., Czurko, A., Mamiya, A., and Buzsaki, G. (1999). Oscillatory coupling of hippocampal pyramidal cells and interneurons in the behaving rat. *J. Neurosci.* 19, 274–287.
- Csicsvari, J., Hirase, H., Mamiya, A., and Buzsaki, G. (2000). Ensemble patterns of hippocampal CA3–CA1 neurons during sharp wave-associated population events. *Neuron* 28, 585–594.

- Draguhn, A., Traub, R.D., Schmitz, D., and Jefferys, J.G. (1998). Electrical coupling underlies high-frequency oscillations in the hippocampus in vitro. *Nature* 394, 189–192.
- Dzhala, V.I., and Staley, K.J. (2004). Mechanisms of fast ripples in the hippocampus. *J. Neurosci.* 24, 8896–8906.
- Esclapez, M., Hirsch, J.C., Ben-Ari, Y., and Bernard, C. (1999). Newly formed excitatory pathways provide a substrate for hyperexcitability in experimental temporal lobe epilepsy. *J. Comp. Neurol.* 408, 449–460.
- Feigenbaum, M.J. (1979). The universal metric properties of nonlinear transformations. *J. Stat. Physiol.* 21, 669–706.
- Foffani, G., Priori, A., Egidi, M., Rampini, P., Tamma, F., Caputo, E., Moxon, K.A., Cerutti, S., and Barbieri, S. (2003). 300-Hz subthalamic oscillations in Parkinson's disease. *Brain* 126, 2153–2163.
- Fox, S.E., and Ranck, J.B., Jr. (1981). Electrophysiological characteristics of hippocampal complex-spike cells and theta cells. *Exp. Brain Res.* 41, 399–410.
- Grenier, F., Timofeev, I., and Steriade, M. (2001). Focal synchronization of ripples (80–200 Hz) in neocortex and their neuronal correlates. *J. Neurophysiol.* 86, 1884–1898.
- Hirsch, J.C., Agassandian, C., Merchan-Perez, A., Ben-Ari, Y., DeFelipe, J., Esclapez, M., and Bernard, C. (1999). Deficit of quantal release of GABA in experimental models of temporal lobe epilepsy. *Nat. Neurosci.* 2, 499–500.
- Jefferys, J.G.R. (1995). Nonsynaptic modulation of neuronal activity in the brain: electric currents and extracellular ions. *Physiol. Rev.* 75, 689–723.
- Jirsch, J.D., Urrestarazu, E., LeVan, P., Olivier, A., Dubeau, F., and Gotman, J. (2006). High-frequency oscillations during human focal seizures. *Brain* 129, 1593–1608.
- Jones, M.S., and Barth, D.S. (1999). Spatiotemporal organization of fast (>200 Hz) electrical oscillations in rat vibrissa/barrel cortex. *J. Neurophysiol.* 82, 1599–1609.
- Kandel, A., and Buzsáki, G. (1997). Cellular-synaptic generation of sleep spindles, spike-and-wave discharges, and evoked thalamocortical responses in the neocortex of the rat. *J. Neurosci.* 17, 6783–6797.
- Khosravani, H., Pinnegar, C.R., Mitchell, J.R., Bardakjian, B.L., Federico, P., and Carlen, P.L. (2005). Increased high-frequency oscillations precede in vitro low-Mg seizures. *Epilepsia* 46, 1188–1197.
- Klee, R., Ficker, E., and Heinemann, U. (1995). Comparison of voltage-dependent potassium currents in rat pyramidal neurons acutely isolated from hippocampal regions CA1 and CA3. *J. Neurophysiol.* 74, 1982–1995.
- Kobayashi, M., and Buckmaster, P.S. (2003). Reduced inhibition of dentate granule cells in a model of temporal lobe epilepsy. *J. Neurosci.* 23, 2440–2452.
- Kubota, D., Colgin, L.L., Casale, M., Brucher, F.A., and Lynch, G. (2003). Endogenous waves in hippocampal slices. *J. Neurophysiol.* 89, 81–89.
- Lopez-Aguado, L., Ibarz, J.M., and Herreras, O. (2001). Activity-dependent changes of tissue resistivity in the CA1 region in vivo are layer-specific: modulation of evoked potentials. *Neuroscience* 108, 249–262.
- Maier, N., Nimmrich, V., and Draguhn, A. (2003). Cellular and network mechanisms underlying spontaneous sharp wave-ripple complexes in mouse hippocampal slices. *J. Physiol.* 550, 873–887.
- Shah, M.M., Anderson, A.E., Leung, V., Lin, X., and Johnston, D. (2004). Seizure-induced plasticity of h channels in entorhinal cortical layer III pyramidal neurons. *Neuron* 44, 495–508.
- Menendez de la Prida, L., and Gal, B. (2004). Synaptic contributions to focal and widespread spatiotemporal dynamics in the isolated rat subiculum in vitro. *J. Neurosci.* 24, 5525–5536.
- Menendez de la Prida, L., Huberfeld, G., Cohen, I., and Miles, R. (2006). Threshold behavior in the initiation of hippocampal population bursts. *Neuron* 49, 131–142.
- Nadler, J.V., Perry, B.W., and Cotman, C.W. (1980). Selective reinnervation of hippocampal area CA1 and the fascia dentata after destruction of CA3–CA4 afferents with kainic acid. *Brain Res.* 182, 1–9.
- O'Neill, J., Senior, T., and Csicsvari, J. (2006). Place-selective firing of CA1 pyramidal cells during sharp wave/ripple network patterns in exploratory behavior. *Neuron* 49, 143–155.
- Pouille, F., and Scanziani, M. (2001). Enforcement of temporal fidelity in pyramidal cells by somatic feed-forward inhibition. *Science* 293, 1159–1163.
- Racine, R.J. (1972). Modification of seizure activity by electrical stimulation. II. Motor seizure. *Electroencephalogr. Clin. Neurophysiol.* 32, 281–294.
- Ranck, J.B., Jr. (1973). Studies on single neurons in dorsal hippocampal formation and septum in unrestrained rats. I. Behavioral correlates and firing repertoires. *Exp. Neurol.* 41, 461–531.
- Shao, L.R., and Dudek, F.E. (2005). Changes in mIPSCs and sIPSCs after kainate treatment: Evidence for loss of inhibitory input to dentate granule cells and possible compensatory responses. *J. Neurophysiol.* 94, 952–960.
- Siddiqui, A.H., and Joseph, S.A. (2005). CA3 axonal sprouting in kainate-induced chronic epilepsy. *Brain Res.* 1066, 129–146.
- Skaggs, W.E., and McNaughton, B.L. (1996). Replay of neuronal firing sequences in rat hippocampus during sleep following spatial experience. *Science* 271, 1870–1873.
- Snow, R.W., and Dudek, F.E. (1986). Evidence for neuronal interactions by electrical field effects in the CA3 and dentate regions of rat hippocampal slices. *Brain Res.* 367, 292–295.
- Somogyi, P., and Klausberger, T. (2005). Defined types of cortical interneurone structure space and spike timing in the hippocampus. *J. Physiol.* 562, 9–26.
- Storm, J.F. (1990). Potassium currents in hippocampal pyramidal cells. *Prog. Brain Res.* 83, 161–187.
- Staley, K.J., Longacher, M., Bains, J.S., and Yee, A. (1998). Presynaptic modulation of CA3 network activity. *Nat. Neurosci.* 1, 201–209.
- Suzuki, S.S., and Smith, G.K. (1988). Spontaneous EEG spikes in the normal hippocampus. II. Relations to synchronous burst discharges. *Electroencephalogr. Clin. Neurophysiol.* 69, 532–540.
- Thompson, S.M., Capogna, M., and Scanziani, M. (1993). Presynaptic inhibition in the hippocampus. *Trends Neurosci.* 16, 222–227.
- Traub, R.D., and Bibbig, A. (2000). A model of high-frequency ripples in the hippocampus based on synaptic coupling plus axon-axon gap junctions between pyramidal neurons. *J. Neurosci.* 20, 2086–2093.
- Traub, R.D., Contreras, D., Cunningham, M.O., Murray, H., LeBeau, F.E., Roopun, A., Bibbig, A., Wilent, W.B., and Higley, M.J. (2005). Whittington MA. Single-column thalamocortical network model exhibiting gamma oscillations, sleep spindles, and epileptogenic bursts. *J. Neurophysiol.* 93, 2194–2232.
- Wilson, M.A., and McNaughton, B.L. (1994). Reactivation of hippocampal ensemble memories during sleep. *Science* 265, 676–679.
- Wong, R.K., and Prince, D.A. (1981). Afterpotential generation in hippocampal pyramidal cells. *J. Neurophysiol.* 45, 86–97.
- Yiinen, A., Bragin, A., Nadasdy, Z., Jando, G., Szabo, I., Sik, A., and Buzsáki, G. (1995). Sharp wave-associated high-frequency oscillation (200 Hz) in the intact hippocampus: network and intracellular mechanisms. *J. Neurosci.* 15, 30–46.